IN-PLANE THERMAL RESIDUAL STRESSES IN ADHESIVELY BONDED FUNCTIONALLY GRADED PLATES

M. Kemal Apalak*[1], M. Didem Demirbas[1]

[1] *Erciyes University, Department of Mechanical Engineering, Kayseri 38039, Turkey*
* *Corresponding Author: apalakmk@erciyes.edu.tr*

Keywords: Functionally graded plate, adhesive joint, thermal residual stress, finite difference method

Abstract
This study addresses the effect of the coordinate derivatives of material properties on the thermal stress and strain states in adhesively bonded in-plane clamped functionally graded joints. The consideration of material derivatives indicates lower stress and strain levels in the functionally graded plates and in the adhesive joints, and that the strain distributions are completely affected whereas the stress distributions remain similar but the size of the high stress regions changes. The adhesive layer is most critical member of adhesively bonded plates since it experiences considerable strains due to thermal mismatches of the adhesive and material composition at both sides of the adhesive interface. The study showed that the consideration of the material derivatives was necessary to calculate correctly the actual stress and strain distributions.

1. Introduction

Thermal and structural loads result in discontinuous stress concentrations along bi-material interfaces of layered composites due to their discontinuous thermal and mechanical properties. In practice, high thermal gradients need to be reduced through thickness of structural member. However, stress and deformation states are affected by thermal and mechanical mismatches between layers. Functionally graded materials achieve a smooth transition among the layers of the composite material [1, 2] by having a continuously varying material composition along one dimension of a structure. The thermal residual stresses induced by processing or in-service thermal conditions or thermal loads under typical edge conditions have been investigated in detail [3, 4, 5, 6, 7, 8, 9, 10, 11, 12, 13] whereas the studies on the effects of the structural loads in functionally graded plates are limited [6-8,14]. A detailed introduction to the fundamentals of functionally graded materials [2] and an extensive review concerned with thermal stress problems are available [3].

The thermoelastic stress analysis of a functionally graded plate using the first-order shear deformation plate theory showed that the thermomechanical coupling played a more important role when the power law exponent is small [6]. The material distribution affects the through-thickness deflections and stress states of functionally graded plates [7]. The assumption of a constant through-thickness deflection is invalid for the functionally graded plates under the thermal loads [8]. The through-thickness material composition variation and the size of the

functionally gradient layer have effects on the thermal stress characteristics [9]. However, the averaging estimation methods of material characteristics produce stress distributions, with considerable difference from those by the finite element discritized models [10, 11].

Apalak et al. investigated the thermoelastic behaviour of functionally graded rectangular plates and adhesively bonded functionally graded rectangular and circular hollow plates for temperature-independent, in-plane, not through-thickness, material composition variations and for an in-plane heat flux [14, 15, 16]. The type of in-plane heat flux had effects on both heat transfer period and temperature levels rather than the in-plane temperature profile, and the residual thermal stresses were strongly dependent on the in-plane material composition gradient, and could be reduced by tailoring in-plane material composition. The two-dimensional heat conduction problem of a thick hollow cylinder with finite length made of 2D-FGM subjected to transient thermal boundary conditions showed that the material distribution in two directions affected both the temperature distribution and time responses of the cylinder [17]. A study on the steady thermal stress problem of 2D-FGM plate having a linear temperature load on its upper surface indicated that the optimization of a 2D-FGM plate is more wide and concrete basis of calculation for design [18, 19]. Nemat-Alla [20] proposed suitable functions representing volume fractions of the 2D-FGMs, and showed that the 2D-FGMs have high capability to reduce thermal stresses. Nemat-Alla et al. [21] also investigated the elastic-plastic stress behaviours of the 2D-FGMs. They proposed a 3D finite element model of the 2D-FGM plates, and found that heat conductivity of the metallic constituents of FGM has a great effect on the temperature distributions. The lower temperature variations and lower stresses can be obtained using the 2D-FGMs without fracture or plastic deformations.

The present thermal stress analyses have concentrated on the one- or two-dimensional functionally graded structures through their thickness. Today's fuel cell technology allows the use of FGMs in solid oxide fuel cells in order to reduce mismatches in the thermal expansion coefficients between electrolyte and anode [22]. Wang et al. [23] presented a comprehensive review on five categories of fuel cells, and related studies. Fuel cells can be designed by considering convective and conductive heat transfers, heat and mass transfer, multiple fluid flows as well as electrochemical reactions [24, 25]. Consequently, a planar design of a solid oxide fuel cell may experience in-plane or through-thickness heat transfer due to heat fluxes. Therefore, the suitability of in-plane one- or two-dimensional functionally graded material distributions requires an theoretical investigation for these types of practical applications.

2. THEORETICAL MODEL AND ANALYSIS

In this paper the functionally graded plate has a material composition with two constituents, ceramic and metal, and its material composition is bi-directional in the plate plane. The determination of the physical/mechanical properties of the material composition at any point, thermal and stress analyses are explained in the following sections:

2.1. Material Properties

In general, a FGM is designed as a layer with continuous composition variation through a direction, especially through-the-thickness, of plate in order to provide high-temperature resistance on one of the plate edges using the low thermal conductivity of ceramic constituent. How-

ever, an actual FGM consists of ceramic and metal particles with arbitrary shapes mixed up in randomly dispersed structures. Thermo-mechanical properties of an FGM are function of this shape and orientation of ceramic and metal particles, the dispersion structure as well as volume fractions. The functionally graded composite plates are designed as a homogeneous isotropic graded layer between ceramic and metal phases. The volume fractions of the ceramic (c) and metal (m) constituents of the plates obey the power law. Thus, the ceramic composition of the lower plate changes from the ceramic-rich to the material-rich as

$$V_c(x,y) = \left(\frac{x}{l}\right)^n \left(1 - \frac{y}{h}\right)^m \tag{1}$$

whereas the ceramic composition of the upper plate changes from the metal-rich to the ceramic-rich as

$$V_c(x,y) = \left(\frac{x}{l}\right)^n \left(\frac{y}{h}\right)^m \tag{2}$$

where n is x- directional compositional gradient exponent, m is y- directional compositional gradient exponent, h is the plate length and l is the plate width (Figure 1). The volume fraction of the metal (m) of the plates changes as

$$V_m(x,y) = 1 - V_c(x,y) \tag{3}$$

The mechanical properties of the FGM are based on the Mori-Tanaka relation [26]. The overall bulk modulus

$$K(x,y) = K_m + \frac{V_c\,(K_c - K_m)}{1 + (1 - V_c)\,\dfrac{3\,(K_c - K_m)}{3K_m + 4G_m}} \tag{4}$$

and the overall shear modulus G is

$$G(x,y) = G_m + \frac{V_c\,(G_c - G_m)}{1 + (1 - V_c)\,\dfrac{G_c - G_m}{G_m + f_1}} \tag{5}$$

and where f_1 is

$$f_1 = \frac{G_m\,(9K_m + 8G_m)}{6\,(K_m + 2G_m)} \tag{6}$$

The overall modulus of elasticity

$$E(x,y) = \frac{9KG}{3K + G} \tag{7}$$

The overall Poisson's ratio is written as

$$\nu(x,y) = \frac{3K - 2G}{2\,(3K + G)} \tag{8}$$

The coefficient of thermal expansion [27]

$$\alpha(x,y) = \alpha_m + (\alpha_c - \alpha_m)\,\frac{K_c\,(K_m - K)}{K\,(K_m - K_c)} \tag{9}$$

The coefficient of thermal conductivity [28]

$$\lambda(x,y) = \lambda_m + V_c\,(\lambda_c - \lambda_m)\left(1 + (1 - V_c)\,\frac{\lambda_c - \lambda_m}{3\lambda_m}\right) \tag{10}$$

The specific heat capacity coefficient [28]

$$c_p\,(x,y) = c_{p_m} + V_c\left(c_{p_c} - c_{p_m}\right)\left(1 + (1 - V_c)\,\frac{c_{p_c} - c_{p_m}}{3c_{p_m}}\right) \tag{11}$$

Using the linear rule of mixtures the density can be written as

$$\rho\,(x,y) = \rho_c V_c + \rho_m V_m \tag{12}$$

2.2. Heat Transfer Model

Transient three-dimensional heat conduction equation is

$$\underset{\sim}{\nabla}\left(\lambda \underset{\sim}{\nabla} T\right) = \rho c_p \frac{\partial T}{\partial t} \tag{13}$$

where λ is heat conductivity coefficient, ρ is density, c_p is specific heat and $\underset{\sim}{\nabla}$ (del) operator. For the two-dimensional (plane) case with dependency on the direction of material derivation

$$\frac{\partial \lambda}{\partial x}\frac{\partial T}{\partial x} + \frac{\partial \lambda}{\partial y}\frac{\partial T}{\partial y} + \lambda\left(\frac{\partial^2 T}{\partial x^2} + \frac{\partial^2 T}{\partial y^2}\right) = \rho c_p \frac{\partial T}{\partial t} \tag{14}$$

The forward and central-difference equations can be applied to the first and second-order derivatives of the temperature $T(x, y, t)$ at the nodal point (i, j) with the coordinate (x, y) or with respect to time t and the space variables (x, y). Similarly, the first order derivatives of the heat conductivity coefficient $\lambda = \lambda(x, y)$ with respect to the space variables (x, y) can be written using the forward- and backward-difference equations. Consequently, the heat transfer equation (14) can be written in terms of difference equations as

$$\begin{aligned} T_{i,j}^{k+1} =& T_{i,j}^{k} + \frac{\Delta t}{(\rho c_p)_{i,j}(\Delta x)^2}\left(\lambda_{i+1,j} - \lambda_{i,j}\right)\left(T_{i+1,j}^{k} - T_{i,j}^{k}\right) \\ &+ \frac{\Delta t}{(\rho c_p)_{i,j}(\Delta y)^2}\left(\lambda_{i,j+1} - \lambda_{i,j}\right)\frac{1}{\Delta y}\left(T_{i,j+1}^{k} - T_{i,j}^{k}\right) \\ &+ (r_x)_{i,j}\left(T_{i+1,j}^{k} - 2T_{i,j}^{k} + T_{i-1,j}^{k}\right) + (r_y)_{i,j}\left(T_{i,j+1}^{k} - 2T_{i,j}^{k} + T_{i,j-1}^{k}\right) \end{aligned} \tag{15}$$

where

$$a_{i,j} = \left.\frac{\lambda}{\rho c_p}\right|_{i,j}, \quad (r_x)_{i,j} = \frac{\Delta t}{\Delta x}a_{i,j}, \quad (r_y)_{i,j} = \frac{\Delta t}{\Delta y}a_{i,j} \tag{16}$$

where Δx, Δy and Δt are space and time increments, respectively. All physical and thermal properties in the coefficients (16) are considered for the present material at the grid point (i, j).

2.3. Implementation of Initial and Boundary Conditions

The initial temperature distribution is given as

$$T(x,y) = 298\ \text{K} \quad \text{at} \quad t = 0 \tag{17}$$

and the thermal boundary conditions are given as

$$q(x, 2h + h_a, t) = q_o \tag{18}$$

where h_a is adhesive thickness, q is a heat flux along the coordinate y respectively, and $q_o = 70$ kW/m^2. The other edges are subjected to adiabatic conditions (Figure 1). The finite difference method requires that the plates be divided into a mesh of nx times ny divisions along the coordinates x and y, respectively. The implementation of the boundary conditions require the heat transfer equations to be written in terms of the heat flux along the bonded-plate edges. Thus, the difference equations can be written as along the edge AB ($i = 1, x = 0$) of the bonded plates

$$T_{i,j}^{k+1} = T_{i,j}^{k} + 2\,(r_x)_{i,j}\left(T_{i+1,j}^{k} - T_{i,j}^{k}\right) + \left(r_y\right)_{i,j}\left(T_{i,j+1}^{k} - T_{i,j}^{k}\right) + \left(r_y\right)_{i,j}\left(T_{i,j-1}^{k} - T_{i,j}^{k}\right) \tag{19}$$

along the edge CD ($i = nx, x = l$) of the bonded plates

$$T_{i,j}^{k+1} = T_{i,j}^{k} + 2\,(r_x)_{i,j}\left(T_{i-1,j}^{k} - T_{i,j}^{k}\right) + \left(r_y\right)_{i,j}\left(T_{i,j+1}^{k} - T_{i,j}^{k}\right) + \left(r_y\right)_{i,j}\left(T_{i,j-1}^{k} - T_{i,j}^{k}\right) \tag{20}$$

along the edge AC ($j = 1, y = 0$) of the bonded plates as

$$T_{i,j}^{k+1} = T_{i,j}^{k} + 2\left(r_y\right)_{i,j}\left(T_{i,j+1}^{k} - T_{i,j}^{k}\right) + (r_x)_{i,j}\left(T_{i+1,j}^{k} - T_{i,j}^{k}\right) + (r_x)_{i,j}\left(T_{i-1,j}^{k} - T_{i,j}^{k}\right) \tag{21}$$

along the edge BD ($j = ny, y = 2h + h_a$) of the bonded plates

$$\begin{aligned} T_{i,j}^{k+1} =& T_{i,j}^{k} + 2\left(r_y\right)_{i,j}\left(T_{i,j-1}^{k} - T_{i,j}^{k}\right) + (r_x)_{i,j}\left(T_{i+1,j}^{k} - T_{i,j}^{k}\right) \\ &+ (r_x)_{i,j}\left(T_{i-1,j}^{k} - T_{i,j}^{k}\right) + 2q_o\left(\frac{r_{ry}}{\lambda}\right)_{i,j} \end{aligned} \tag{22}$$

at the corner A ($i = 1, j = 1$), ($x = 0, y = 0$)

$$T_{i,j}^{k+1} = T_{i,j}^{k} + 2\,(r_x)_{i,j}\,(T_{i+1,j}^{k} - T_{i,j}^{k}) + 2\left(r_y\right)_{i,j}\left(T_{i,j+1}^{k} - T_{i,j}^{k}\right) \tag{23}$$

at the corner B ($i = 1, j = ny$), ($x = 0, y = 2h + h_a$)

$$T_{i,j}^{k+1} = T_{i,j}^{k} + 2\,(r_x)_{i,j}\left(T_{i+1,j}^{k} - T_{i,j}^{k}\right) + 2\left(r_y\right)_{i,j}\left(T_{i,j-1}^{k} - T_{i,j}^{k}\right) + 2q_o\left(\frac{r_{ry}}{\lambda}\right)_{i,j} \tag{24}$$

at the corner C ($i = nx, j = 1$), ($x = l, y = 0$)

$$T_{i,j}^{k+1} = T_{i,j}^{k} + 2\,(r_x)_{i,j}\left(T_{i-1,j}^{k} - T_{i,j}^{k}\right) + 2\left(r_y\right)_{i,j}\left(T_{i,j+1}^{k} - T_{i.j}^{k}\right) \tag{25}$$

at the corner D ($i = nx, j = ny$), ($x = l, y = 2h + h_a$)

$$T_{i,j}^{k+1} = T_{i,j}^{k} + 2\,(r_x)_{i,j}\left(T_{i-1,j}^{k} - T_{i,j}^{k}\right) + 2\left(r_y\right)_{i,j}\left(T_{i,j-1}^{k} - T_{i,j}^{k}\right) + 2q_o\left(\frac{r_{ry}}{\lambda}\right)_{i,j} \tag{26}$$

where

$$(r_{ry})_{i,j} = \frac{\Delta t}{\Delta y} a_{i,j} \tag{27}$$

Now, the temperatures for the next time step $t + \Delta t$ from temperatures at the time t can be calculated explicitly using equation (15) at the internal points and equations (19)-(26) at the boundary points along the plate edges and at the corners.

2.4. Elasticity Equations

The stress-strain equations are

$$\sigma_{ij} = 2\mu e_{ij} + \lambda\delta_{ij}e_v - \delta_{i,j}\left(3\lambda + 2\mu\right)\alpha\left(\Delta T\right) \tag{28}$$

where $\delta_{i,j}$ is kronecker's delta, α is coefficient of thermal expansion, ΔT is temperature change and Lamé's constants are

$$\lambda = \frac{\nu E}{\left(1+\nu\right)\left(1-2\nu\right)} \tag{29}$$

$$\mu = \frac{E}{2\left(1+\nu\right)} \tag{30}$$

$\nu = \nu(x_1, x_2)$ and $E = E(x_1, x_2)$ are the Poisson's ratio and the modulus of elasticity of the material, respectively, and the volumetric strain is

$$e_v = e_{nn} = e_{11} + e_{22} + e_{33} \tag{31}$$

The strain-displacement equations are

$$e_{ij} = \frac{1}{2}\left(\frac{\partial u_i}{\partial x_j} + \frac{\partial u_j}{\partial x_i}\right) \tag{32}$$

The equilibrium equations are

$$\frac{\partial \sigma_{ij}}{\partial x_j} + F_i = 0 \tag{33}$$

This equations can be reduced to three equations in terms of displacement components by substituting (28) - (32) into (33), and we obtain Navier's equations of elasticity as

$$\frac{\partial}{\partial x_j}\left(2\mu e_{ij} + \lambda\delta_{ij}e_v - \delta_{i,j}\left(3\lambda + 2\mu\right)\alpha\left(\Delta T\right)\right) + F_i = 0 \tag{34}$$

For two-dimensional elasticity problems let $x = x_1$ and $y = x_2$ and $u = u_1(x_1, x_2)$, $v = u_2(x_1, x_2)$, with $\mu = \mu(x, y)$, $\lambda = \lambda(x, y)$ and $\alpha = \alpha(x, y)$, the elasticity equations (34) in terms of the displacements in the absence of the body forces ($F_i = 0$) can be written explicitly as

$$\begin{aligned} &2\frac{\partial\mu}{\partial x}\frac{\partial u}{\partial x} + \frac{\partial\mu}{\partial y}\left(\frac{\partial u}{\partial y} + \frac{\partial v}{\partial x}\right) + \frac{\partial\lambda}{\partial x}\left(\frac{\partial u}{\partial x} + \frac{\partial v}{\partial y}\right) \\ &+ \left(\lambda + 2\mu\right)\frac{\partial^2 u}{\partial x^2} + \left(\lambda + \mu\right)\frac{\partial^2 v}{\partial y \partial x} + \mu\frac{\partial^2 u}{\partial y^2} - 3\alpha\bar{T}\frac{\partial\lambda}{\partial x} \\ &-2\alpha\bar{T}\frac{\partial\mu}{\partial x} - \left(3\lambda + 2\mu\right)\bar{T}\frac{\partial\alpha}{\partial x} - \left(3\lambda + 2\mu\right)\alpha\frac{\partial\bar{T}}{\partial x} = 0 \end{aligned} \tag{35}$$

$$\begin{aligned} &2\frac{\partial\mu}{\partial y}\frac{\partial v}{\partial y} + \frac{\partial\mu}{\partial x}\left(\frac{\partial v}{\partial x} + \frac{\partial u}{\partial y}\right) + \frac{\partial\lambda}{\partial y}\left(\frac{\partial u}{\partial x} + \frac{\partial v}{\partial y}\right) \\ &+ \left(\lambda + 2\mu\right)\frac{\partial^2 v}{\partial y^2} + \left(\lambda + \mu\right)\frac{\partial^2 u}{\partial x \partial y} + \mu\frac{\partial^2 v}{\partial x^2} - 3\alpha\bar{T}\frac{\partial\lambda}{\partial y} \\ &-2\alpha\bar{T}\frac{\partial\mu}{\partial y} - \left(3\lambda + 2\mu\right)\bar{T}\frac{\partial\alpha}{\partial y} - \left(3\lambda + 2\mu\right)\alpha\frac{\partial\bar{T}}{\partial y} = 0 \end{aligned} \tag{36}$$

where $T_f = 298$ K and $\bar{T} = \Delta T(x,y) = T(x,y) - T_f$.

The adhesive layer is homogeneous and the material constants are not function of spatial coordinates (x,y), consequently their coordinate derivatives become zero. The elasticity equations (35 and 36) in terms of displacement components become

$$(\lambda + 2\mu)\frac{\partial^2 u}{\partial x^2} + (\lambda + \mu)\frac{\partial^2 v}{\partial y \partial x} + \mu\frac{\partial^2 u}{\partial y^2} - (3\lambda + 2\mu)\alpha\frac{\partial \bar{T}}{\partial x} = 0 \tag{37}$$

$$(\lambda + 2\mu)\frac{\partial^2 v}{\partial y^2} + (\lambda + \mu)\frac{\partial^2 u}{\partial x \partial y} + \mu\frac{\partial^2 v}{\partial x^2} - (3\lambda + 2\mu)\alpha\frac{\partial \bar{T}}{\partial y} = 0 \tag{38}$$

The first- and second-order derivatives of displacement components $u(x,y)$ and $v(x,y)$ with respect to space variables (x,y), and the first-order derivatives of the material constants and temperature difference can be expressed using the suitable central, backward or forward difference equations for the internal points of the plate. Therefore, the elasticity equations in terms of displacements can be written as

$$\begin{aligned}
&2\frac{\mu_{i+1,j} - \mu_{i,j}}{\Delta x}\left(\frac{u_{i+1,j} - u_{i,j}}{\Delta x}\right) + \frac{\mu_{i,j+1} - \mu_{i,j}}{\Delta y}\left(\frac{u_{i,j+1} - u_{i,j}}{\Delta y} + \frac{v_{i+1,j} - v_{i,j}}{\Delta x}\right) \\
&+\frac{\lambda_{i+1,j} - \lambda_{i,j}}{\Delta x}\left(\frac{u_{i+1,j} - u_{i,j}}{\Delta x} + \frac{v_{i,j+1} - v_{i,j}}{\Delta y}\right) + (\lambda + 2\mu)\frac{u_{i+1,j} - 2u_{i,j} + u_{i-1,j}}{(\Delta x)^2} \\
&+(\lambda + \mu)\frac{v_{i+1,j+1} - v_{i+1,j} - v_{i,j+1} + v_{i,j}}{\Delta y \Delta x} + \mu\frac{u_{i,j+1} - 2u_{i,j} + u_{i,j-1}}{(\Delta y)^2} - 3\alpha\bar{T}\frac{\lambda_{i+1,j} - \lambda_{i,j}}{\Delta x} \\
&-2\alpha\bar{T}\frac{\mu_{i+1,j} - \mu_{i,j}}{\Delta x} - (3\lambda + 2\mu)\bar{T}\frac{\alpha_{i+1,j} - \alpha_{i,j}}{\Delta x} - (3\lambda + 2\mu)\alpha\frac{\bar{T}_{i+1,j} - \bar{T}_{i,j}}{\Delta x} = 0
\end{aligned} \tag{39}$$

and

$$\begin{aligned}
&2\frac{\mu_{i,j+1} - \mu_{i,j}}{\Delta y}\left(\frac{v_{i,j+1} - v_{i,j}}{\Delta y}\right) + \frac{\mu_{i+1,j} - \mu_{i,j}}{\Delta x}\left(\frac{v_{i+1,j} - v_{i,j}}{\Delta x} + \frac{u_{i,j+1} - u_{i,j}}{\Delta y}\right) \\
&+\frac{\lambda_{i,j+1} - \lambda_{i,j}}{\Delta y}\left(\frac{u_{i+1,j} - u_{i,j}}{\Delta x} + \frac{v_{i,j+1} - v_{i,j}}{\Delta y}\right) + (\lambda + 2\mu)\frac{v_{i,j+1} - 2v_{i,j} + v_{i,j-1}}{(\Delta y)^2} \\
&+(\lambda + \mu)\frac{u_{i+1,j+1} - u_{i+1,j} - u_{i,j+1} + u_{i,j}}{\Delta x \Delta y} + \mu\frac{v_{i+1,j} - 2v_{i,j} + v_{i-1,j}}{(\Delta x)^2} - 3\alpha\bar{T}\frac{\lambda_{i,j+1} - \lambda_{i,j}}{\Delta y} \\
&-2\alpha\bar{T}\frac{\mu_{i,j+1} - \mu_{i,j}}{\Delta y} - (3\lambda + 2\mu)\bar{T}\frac{\alpha_{i,j+1} - \alpha_{i,j}}{\Delta y} - (3\lambda + 2\mu)\alpha\frac{\bar{T}_{i,j+1} - \bar{T}_{i,j}}{\Delta y} = 0
\end{aligned} \tag{40}$$

For the adhesive layer, the discretizated elasticity equations can be written as

$$\begin{aligned}
&(\lambda + 2\mu)\frac{u_{i+1,j} - 2u_{i,j} + u_{i-1,j}}{(\Delta x)^2} + (\lambda + \mu)\frac{v_{i+1,j+1} - v_{i+1,j} - v_{i,j+1} + v_{i,j}}{\Delta y \Delta x} \\
&+\mu\frac{u_{i,j+1} - 2u_{i,j} + u_{i,j-1}}{(\Delta y)^2} - (3\lambda + 2\mu)\alpha\frac{\bar{T}_{i+1,j} - \bar{T}_{i,j}}{\Delta x} = 0
\end{aligned} \tag{41}$$

and

$$\begin{aligned}
&(\lambda + 2\mu)\frac{v_{i,j+1} - 2v_{i,j} + v_{i,j-1}}{(\Delta y)^2} + (\lambda + \mu)\frac{u_{i+1,j+1} - u_{i+1,j} - u_{i,j+1} + u_{i,j}}{\Delta x \Delta y} \\
&+\mu\frac{v_{i+1,j} - 2v_{i,j} + v_{i-1,j}}{(\Delta x)^2} - (3\lambda + 2\mu)\alpha\frac{\bar{T}_{i,j+1} - \bar{T}_{i,j}}{\Delta y} = 0
\end{aligned} \tag{42}$$

2.5. Implementation of Boundary Conditions

All four edges of the bonded plates are clamped as

$$u(x, y) = 0 \tag{43}$$
$$v(x, y) = 0 \tag{44}$$

These boundary conditions can be implemented using each of backward- or central- difference schemes. Let one of the displacement components $u(x, y)$ and $v(x, y)$ be represented $\psi = \psi(x, y)$, the difference equations of their partial derivatives with respect to the space variables x and y at the grid nodes along the four edges can be written as

$$\frac{\partial \psi}{\partial x} = \frac{\psi_{i,j} - \psi_{i-1,j}}{\Delta x} \tag{45}$$
$$\frac{\partial \psi}{\partial y} = \frac{\psi_{i,j} - \psi_{i,j-1}}{\Delta y} \tag{46}$$

$$\frac{\partial^2 \psi}{\partial x^2} = \frac{-\psi_{i+3,j} + 4\psi_{i+2,j} - 5\psi_{i+1,j} + 2\psi_{i,j}}{(\Delta x)^2} \tag{47}$$
$$\frac{\partial^2 \psi}{\partial x^2} = \frac{-\psi_{i-3,j} + 4\psi_{i-2,j} - 5\psi_{i-1,j} + 2\psi_{i,j}}{(\Delta x)^2} \tag{48}$$
$$\frac{\partial^2 \psi}{\partial y^2} = \frac{-\psi_{i,j+3} + 4\psi_{i,j+2} - 5\psi_{i,j+1} + 2\psi_{i,j}}{(\Delta y)^2} \tag{49}$$
$$\frac{\partial^2 \psi}{\partial y^2} = \frac{-\psi_{i,j-3} + 4\psi_{i,j-2} - 5\psi_{i,j-1} + 2\psi_{i,j}}{(\Delta y)^2} \tag{50}$$
$$\frac{\partial^2 \psi}{\partial x \partial y} = \frac{\psi_{i+1,j+1} - \psi_{i+1,j} - \psi_{i,j+1} + \psi_{i,j}}{\Delta x \Delta y} \tag{51}$$
$$\frac{\partial^2 \psi}{\partial x \partial y} = \frac{\psi_{i,j+1} - \psi_{i,j} - \psi_{i-1,j+1} + \psi_{i-1,j}}{\Delta x \Delta y} \tag{52}$$
$$\frac{\partial^2 \psi}{\partial x \partial y} = \frac{\psi_{i,j} - \psi_{i,j-1} - \psi_{i-1,j} + \psi_{i-1,j-1}}{\Delta x \Delta y} \tag{53}$$
$$\frac{\partial^2 \psi}{\partial x \partial y} = \frac{\psi_{i+1,j} - \psi_{i+1,j-1} - \psi_{i,j} + \psi_{i,j-1}}{\Delta x \Delta y} \tag{54}$$

Let $\phi = \phi(x, y)$ to be the temperature change $\bar{T}$ or one of material properties (λ, μ, α). The backward-difference equations of their first order derivatives at the node (i, j) with respect to the space variables (x, y)

$$\frac{\partial \phi}{\partial x} = \frac{\phi_{i,j} - \phi_{i-1,j}}{\Delta x} \tag{55}$$
$$\frac{\partial \phi}{\partial y} = \frac{\phi_{i,j} - \phi_{i,j-1}}{\Delta y} \tag{56}$$

Navier's equations (35) and (36) can be reduced to a system of linear equations in terms of two displacement components by substituting equations (41)-(42) at the internal points as well as equations (45)-(56) at the boundary points.

The system of linear equations can be resolved into the form $[C]\{u\} = [B]$. The sparse matrix of coefficients is singular; consequently, the system of linear equations can be solved for the displacement components using the pseudo singular value methods. The explicit difference equations of the thermal analysis and the implicit difference equations of the stress analysis are coded, solved and post-processed graphically in MATLAB mathematical software [29].

3. Results

In this study the thermoelastic stress analysis of adhesively bonded bi-directional functionally graded plates was carried out based on two-dimensional elasticity equations. The functionally graded plates have a width of $h = 48$ mm, a length of $l = 100$ mm and a thickness of $t = 1$ mm, respectively. The adhesive thickness is taken as $t_a = 4$ mm. The property distribution of the ceramic and metal composition is designed in the plate plane rather than through the plate thickness (Figure 1). The in-plane material composition obeys the composition variation rule defined by equations (1 and 2). Thus, the edges of the lower and upper plates contacting with the adhesive layer are pure metal whereas their other edges AC and BD are pure ceramic. The mechanical and physical properties of the ceramic and metal constituents and epoxy adhesive are given in Table 1. A constant in-plane heat flux $q(t) = 70\ \mathrm{kW/m^2}$ was applied along the pure ceramic edge BD of the upper plate whereas an adiabatic condition is assumed for other edges. The compositional gradient exponents n and m are related to the composition variations in the x and $y-$directions, respectively, and considered as 0.1, 0.2 and 0.3. The initial temperature distributions is assumed to be uniform in the plates and in the adhesive layer at a temperature of 298 K. The plate edges are clamped applying $u(x, y) = 0$ and $v(x, y) = 0$. The thermal analysis was ended when the temperature at a grid point in the adhesive layer having coordinates $(x = \frac{l}{2}, y = h + \frac{t_a}{2})$ reached a temperature of 393 K. After the thermal analysis was completed the temperature distribution at the final time step was used in the thermal stress analysis. The different in-plane material composition variations, and the space derivatives of the mechanical properties of the material composition were considered and their effects on the equivalent strain and stress in-plane distributions were investigated.

Figure 2 shows the effect of compositional gradient exponents (n) and (m) in the $x-$ and $y-$ directions on the equivalent strain $\varepsilon_{eqv}(x, y)$ distributions in the upper functionally graded plate based on the thermal stress analyses by/without considering the spatial coordinate derivations of the material constants (λ, μ, α). Each of the compositional gradient exponents (n) and (m) is kept constant at a value of 0.1, respectively and the other exponent is changed as $0.1, 0.2$ and 0.3 in order to determine the effect of the active compositional gradient exponent. In case the gradient exponent $m = 0.1$ indicating the composition variation along the $y-$direction the equivalent strain $\varepsilon_{eqv}(x, y)$ distributions are similar for the gradient exponent values $(n = 0.1, 0.2, 0.3)$ indicating the composition variation along the $x-$direction. The middle region of the pure-ceramic edge, the left and right edges of the pure-metal region bonded to the adhesive layer experience high strain levels $(5 - 7 \times 10^{-4})$ whereas the middle region undergoes negligible equivalent strains. The consideration of the material derivatives indicates a decrease in the peak equivalent levels (from 7 to 5.8×10^{-4}) and a narrow peak strain region along the pure ceramic edge as the gradient exponent n is increased. The analyses without the material derivations predict higher equivalent strain levels (9×10^{-4}) and a larger high strain region around the pure ceramic edge. Negligible differences are observed for strain distributions and levels as the composition gradient n is increased. The analysis with material derivatives (MDRV) predicts

that as the heat flux is applied in the y-direction an effective composition variation along the x-direction reduces peak strain levels, but the analysis without material derivatives (NMDRV) predicts almost similar distributions and levels. In case the gradient exponent $n = 0.1$ indicating the composition variation along the $x-$direction the equivalent strain distributions are similar for the gradient exponent values ($m = 0.1, 0.2, 0.3$) indicating the composition variation along the $y-$direction. The analysis (MDRV) indicates a narrower region having lower strain levels than those of the analysis (NMDRV). However, the composition variation along the y-direction has negligible effect, and the analysis indicates increases in the peak strain levels.

Figure 3 shows the effects of the compositional gradient exponents and the consideration of material derivations on the equivalent stress $\sigma_{eqv}(x, y)$ distributions. The gradient exponent n, as $m = 0.1$ is constant, changes the ceramic composition; therefore, the high stress regions exhibit different distributions concentrating around the pure ceramic plate corner and the size of these regions get narrower. However, the peak stress levels are affected negligibly. The analysis (MDRV) predicts larger high stress regions than those of the analysis (NMDRV). In case the gradient exponent m changes as $n = 0.1$ is constant the similar stress distributions are observed and the peak stress levels remain same. However, the high stresses concentrate around the pure ceramic corner of the plate and a narrower and region near the ceramic rich edge of the plate. Therefore, both the gradient exponents can be adjusted in order to control the size of high stress regions, but the peak stress levels.

The effects of the compositional gradient exponents and the consideration of material derivations on the equivalent strain $\varepsilon_{eqv}(x, y)$ distributions are shown in Figure 4. In general the adhesive layer is assumed to be a weak member of the adhesive joints. The free edges of the adhesive layer undergo higher strains whereas the most region of the adhesive layer still experiences negligible strain levels. The analysis (MDRV) predicts high strains at the free edges of the adhesive layer but peak strain levels appearing around the free edges of the adhesive-upper plate interface. However, the analysis (NMDRV) indicates high strains in a larger region with uniform width at the free edges of the adhesive layer. Increasing the gradient exponent n as $m = 0.1$ results in decreases in the peak strain levels (8.2 to 6.8×10^{-4}, MDRV) whereas the analysis (NMDRV) shows negligible changes in the peak strain levels. In case the gradient exponent m changes as $n = 0.1$ the strain distributions and levels are similar, and the analysis (MDRV) indicates decreases in the strain levels with increasing gradient exponent m whereas the analysis (NMDRV) implies increases in strain levels. Increasing the compositional gradient exponent n in the x-direction is more effective on reducing peak adhesive strains.

Figure 5 shows the equivalent stress $\sigma_{eqv}(x, y)$ distributions in the adhesive layer for different compositional gradient exponents based on both analyses (MDRV and NMDRV). The equivalent stresses distribute at the levels of 24.5-27 MPa and the analysis (MDRV) indicates a large region having high stress levels between the upper plate-adhesive interface and the lower plate-adhesive interface from the right free edges of the adhesive layer. In case $m = 0.1$ increasing the gradient exponent n in the x-direction results in small decreases at stress levels but reduces considerably the size of the region elapsed by high stresses. The analysis (MDRV) predicts larger size of high stress region whereas the analysis predicts a very thin strip region with high stress levels. In case $n = 0.1$ increasing the gradient exponent m in the y-direction results in a similar effect of reducing the stress levels in the adhesive layer. The analysis (NMDRV) indicates lower stress levels in a thin region around the right free edge of the adhesive layer.

Figure 6 shows the effects of the compositional gradient exponents (n, m) on the equivalent strain $\varepsilon_{eqv}(x, y)$ distributions in the lower functionally graded plate based on both analyses (MDRV,NMDRV). The equivalent strain concentrates in vicinities of the lower plate-adhesive interface, and becomes peak at the left and right free ends of this interface. The remaining regions of the plate experiences negligible strain levels which are lower than those in the upper functionally graded plate (Figure 2). The analysis (NMDRV) predicts large strain concentration regions around the left and right free ends of the plate-adhesive interface, and the strain levels are nearly twice those predicted by the analysis (MDRV). The analysis (MDRV) aslo indicates that increasing the gradient exponent (n) in the y-direction as $m = 0.1$ results in decreases in the strain levels, however increasing the gradient exponent (m) in the x-direction as $n = 0.1$ results in a contrary effect, thus, increases the strain levels.

The equivalent stress $\sigma_{eqv}(x, y)$ distributions are critical around the plate-adhesive interface and especially in the vicinities of the right free edge of the interface (Figure 7). The stress levels are between 150-380 MPa and are lower than those in the upper functionally graded plate (Figure 3). The analysis (NMDRV) predicts a large region of high stress levels and higher stresses than the analysis (MDRV). The size of the high stress regions remains almost same (NMDRV) whereas increasing gradient exponent (n) in the x-coordinate, while $(m = 0.1)$, results in smaller high stress regions (MDRV). In addition, increasing gradient exponent (m) in the y-coordinate, while $(n = 0.1)$, results in larger high stress regions (MDRV) by reducing the stress levels. However, the size of high stress regions is not affected with increasing gradient exponent m (NMDRV).

Figures 8 and 9 show the effects of the compositional gradient exponents (n, m) on the equivalent stress $\sigma_{eqv}(x, y)$ and the equivalent strain $\varepsilon_{eqv}(x, y)$ variations along the upper plate-adhesive interface, the mid-line of the adhesive layer, and the lower plate-adhesive interface, respectively based on the analyses MDRV and NMDRV. The peak adhesive stresses appear near the right free edge of the adhesive layer (Figure 8). Increasing the gradient exponent (n) for $m = 0.1$ reduces the equivalent stresses and changes the stress variation profiles. The analyses MDRV and NMDRV predict different stress variations but the stress levels are slightly higher for MDRV. However, increasing the gradient exponent (m) for $n = 0.1$ does not provide decreases in the stress levels, on the contrary they are slightly increased with increasing gradient exponent m. A small benefit for adhesive stresses is gained by controlling the material composition variation of the bonded functionally graded plates. However, it is still possible to reduce thermal stresses in the adhesive layer. The equivalent strain is very low in the middle of the adhesive layer, increases towards both free edges of the adhesive layer and becomes peak. The peak equivalent strains at the right free edge of the adhesive layer are higher (Figure 9). The upper interface experiences higher strain levels whereas the lowest strains are observed along the lower interface. The analysis (MDRV) indicates decreases at the equivalent strain levels in the middle of the adhesive layer as the gradient exponent n is increased for a constant $m = 0.1$. However, the analysis (MDRV) predicts a smooth strain variation along the overlap region which becomes minimum in the middle of adhesive layer and peak at both free edges of the adhesive layer, and any change in the strain levels are not observed with increasing the gradient exponent n. Similar results are observed in case the gradient exponent m is increased for a constant $n = 0.1$, but the strain levels are slightly increased in the middle of the adhesive layer whereas the peak strain levels are not affected.

Figures 10 and 11 show the effects of the compositional gradient exponents (n, m) on the equivalent stress $\sigma_{eqv}(x, y)$ and the equivalent strain $\varepsilon_{eqv}(x, y)$ variations along the left edge, the mid-line and the right edge of the adhesively bonded functionally graded plates, respectively based on the analyses MDRV and NMDRV. The lower stresses occur along the left edge and increase towards the right edge (Figure 10). Increasing the gradient exponent n for $m = 0.1$ results in small decreases in the stress levels. The mechanical properties of the functionally graded plates and the adhesive layer play important role on the stress variations. Thus, the adhesive layer experiences lowest stress levels in comparison with those in the plates due to their elastic properties of the local material distribution. Both analyses predict similar stress variations, but the stress levels are predicted higher by the analysis (NMDRV). Similar stress variations are observed as the gradient exponent m is increased for $n = 0.1$ by both analyses (MDRV, NMDRV). Increasing the gradient exponent m provides small decreases along the right edge of the joint, but it causes small increases along the left edge and the mid-line of the joint. The analysis (NMDRV) still predicts stresses higher than the analysis (MDRV). The stress discontinuity along the plate-adhesive interfaces are still present due to the different mechanical properties at both sides of the interfaces. The adhesive layer experiences largest equivalent strains. The left and right-edges of the joint undergo negligible strain levels which are increasing towards the adhesive layer. This is a natural result of the thermal-expansion mismatches between the adhesive and material compositions at both sides of the interfaces. Both analyses predict different equivalent strain variations. However, the strains are lowest at both the left and right edges and highest in the middle of joint based on both analyses. The analysis (NMDRV) gives higher strains. Increasing the gradient exponent n for $m = 0.1$ results in small decreases whereas the gradient exponent m exhibits a contrary effect.

4. Conclusions

The thermal stress analyses of adhesively bonded in-plane clamped functionally graded joints were carried out by considering the coordinate derivatives of material properties. The analysis with material derivatives indicated lower stress and strain levels in the functionally graded plates and in the adhesive joints. The strain distributions were completely affected by the material derivatives whereas the stress distributions remain similar but the size of the high stress regions reduced. The adhesive layer is most critical member of adhesive joint since it experiences considerable strains due to thermal mismatches of the adhesive and material composition at both side of the adhesive interface. The study showed that the consideration of the material derivatives were necessary to predict correctly the actual stress and strain distributions.

References

[1] M. Koizumi. FGM activities in Japan. *Composites Part B: Engineering*, 28(1-2):1 – 4, 1997.

[2] S. Suresh and A. Mortensen. *Fundamentals of Functionally Graded Materials*. The Institute of Materials, London, 1998.

[3] N. Noda. Thermal stresses in functionally graded materials. *Journal of Thermal Stresses*, 22(4-5):477–512, 1999.

[4] L. L. Shaw. Thermal residual stresses in plates and coatings composed of multi-layered

and functionally graded materials. *Composites Part B: Engineering*, 29(3):199 – 210, 1998.

[5] J. Aboudi, M.-J. Pindera, and S.M. Arnold. Higher-order theory for functionally graded materials. *Composites Part B: Engineering*, 30(8):777 – 832, 1999.

[6] J. N. Reddy and C. D. Chin. Thermomechanical analysis of functionally graded cylinders and plates. *Journal of Thermal Stresses*, 21(6):593–626, 1998.

[7] J. N. Reddy. Analysis of functionally graded plates. *International Journal for Numerical Methods in Engineering*, 47(1-3):663–684, 2000.

[8] J.N. Reddy and Z.Q. Cheng. Three-dimensional thermomechanical deformations of functionally graded rectangular plates. *European Journal of Mechanics - A/Solids*, 20(5):841 – 855, 2001.

[9] J.R. Cho and J.Tinsley Oden. Functionally graded material: a parametric study on thermal-stress characteristics using the Crank-Nicolson-Galerkin scheme. *Computer Methods in Applied Mechanics and Engineering*, 188(1-3):17 – 38, 2000.

[10] J.R. Cho and D.Y. Ha. Averaging and finite-element discretization approaches in the numerical analysis of functionally graded materials. *Materials Science and Engineering: A*, 302(2):187 – 196, 2001.

[11] J.R. Cho and D.Y. Ha. Volume fraction optimization for minimizing thermal stress in Ni-Al_2O_3 functionally graded materials. *Materials Science and Engineering: A*, 334(1-2):147 – 155, 2002.

[12] T.L. Becker Jr., R.M. Cannon, and R.O. Ritchie. An approximate method for residual stress calculation in functionally graded materials. *Mechanics of Materials*, 32(2):85 – 97, 2000.

[13] T. Lidong and L. Wenchao. Residual stress analysis of Ti-ZrO_2 thermal barrier graded materials. *Materials and Design*, 23(7):627 – 632, 2002.

[14] M. Kemal Apalak and M. Didem Bagci. Thermal residual stresses in adhesively bonded in-plane functionally graded clamped plates subjected to an edge heat flux. *Journal of Adhesion Science and Technology*, 25(15):1861–1908, 2011.

[15] M. Didem Bagci and M. Kemal Apalak. Thermal residual stresses in one-directional functionally graded plates subjected to in-plane heat flux. *Numerical Heat Transfer, Part A: Applications*, 60(1):50–83, 2011.

[16] M. Kemal Apalak and M. Didem Demirbas. Thermal residual stresses in adhesively bonded in-plane functionally graded clamped circular hollow plates. *Journal of Adhesion Science and Technology*, 27(14):1590–1623, 2013.

[17] M. Asgari and M. Akhlaghi. Transient heat conduction in two-dimensional functionally graded hollow cylinder with finite length. *Heat and Mass Transfer*, 45(11):1383–1392, 2009.

[18] Y.J. Xu and H.Y. Du L.L. Wang and. Analysis of heating steady temperature field in an Al1100/Ti-6Al-4V/SiC 2D-FGM plane plate by FEM. *Key Engineering Materials*, 450:235–238, November 2010.

[19] Y.J. Xu, L.L. Wang, and L.W. Dong. Heating steady thermal stresses in an Al1100/Ti-6Al-4V/SiC 2D-FGM plane four-side clamped plate. *Key Engineering Materials*, 467-469:48–51, February 2011.

[20] Mahmoud Nemat-Alla. Reduction of thermal stresses by developing two-dimensional functionally graded materials. *International Journal of Solids and Structures*, 40(26):7339 – 7356, 2003.

[21] Mahmoud Nemat-Alla, Khaled I.E. Ahmed, and Ibraheem Hassab-Allah. Elastic-plastic analysis of two-dimensional functionally graded materials under thermal loading. *International Journal of Solids and Structures*, 46(14-15):2774 – 2786, 2009.

[22] C. Iwasawa, M. Nagata, Y. Seino, and M. Ono. A study on anode materials and structures for SOFC. volume 97(40) of *Proceedings-Electrochemical Society PV*, pages 626–634, Aachen, Germany, 1997. Electrochemical Society.

[23] Y. Wang, K. S. Chen, J. Mishler, S. C. Cho, and X. C. Adroher. A review of polymer electrolyte membrane fuel cells: Technology, applications, and needs on fundamental research. *Applied Energy*, 88(4):981 – 1007, 2011.

[24] S. Kakac, A. Pramuanjaroenkij, and X. Y. Zhou. A review of numerical modeling of solid oxide fuel cells. *International Journal of Hydrogen Energy*, 32(7):761 – 786, 2007.

[25] A.J Ruys, E.B Popov, D Sun, J.J Russell, and C.C.J Murray. Functionally graded electrical/thermal ceramic systems. *Journal of the European Ceramic Society*, 21(10-11):2025 – 2029, 2001.

[26] T. Mori and K. Tanaka. Average stress in matrix and average elastic energy of materials with misfitting inclusions. *Acta Metallurgica*, 21(5):571 – 574, 1973.

[27] B.Walter Rosen and Zvi Hashin. Effective thermal expansion coefficients and specific heats of composite materials. *International Journal of Engineering Science*, 8(2):157 – 173, 1970.

[28] H. Hatta and M. Taya. Effective thermal conductivity of a misoriented short fiber composite. *Journal of Applied Physics*, 58(7), 1985.

[29] MATLAB R2006b. The Language of Technical Computing. See also URL `http://www.mathworks.com/`, 2012.

Property	**Unit**	**Ni**	**Al_20_3**	**Adhesive**
Density, ρ	kg/m^3	8880	3960	1640
Thermal conductivity, k	W/m-K	60.5×10^{-3}	46×10^{-3}	8.1×10^{-3}
Specific heat capacity, c_p	W-h/kg-K	0.11	0.21	0.16
Shear modulus, G	GPa	76	150	1.638
Bulk modulus, K	GPa	180	172	4.574
Coefficient of thermal expansion, α	1/°C	6.6×10^{-6}	8.1×10^{-6}	40.47×10^{-6}

Table 1. Thermal, physical and mechanical properties of metal (Ni), ceramic (Al_20_3) and adhesive.

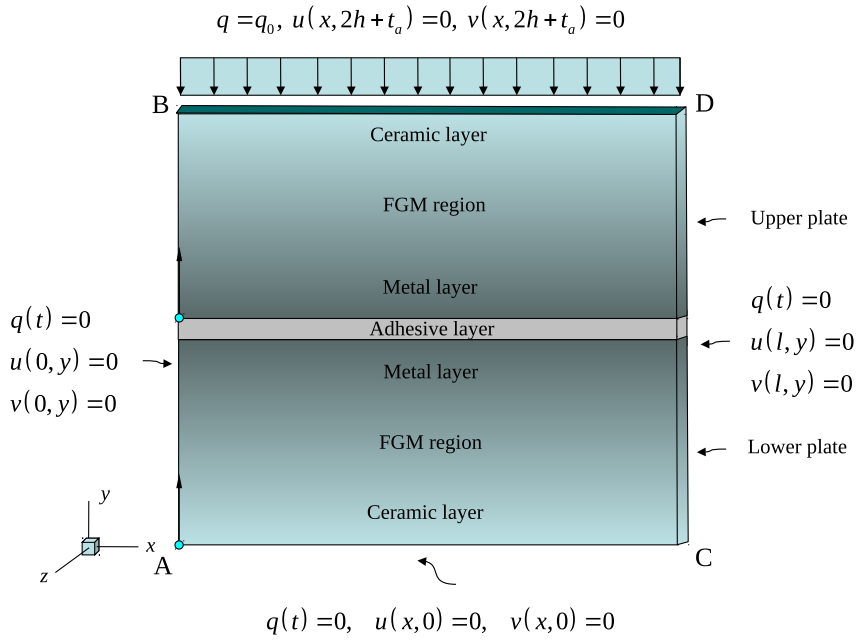

Figure 1. Boundary conditions and geometry of adhesively bonded functionally graded plates.

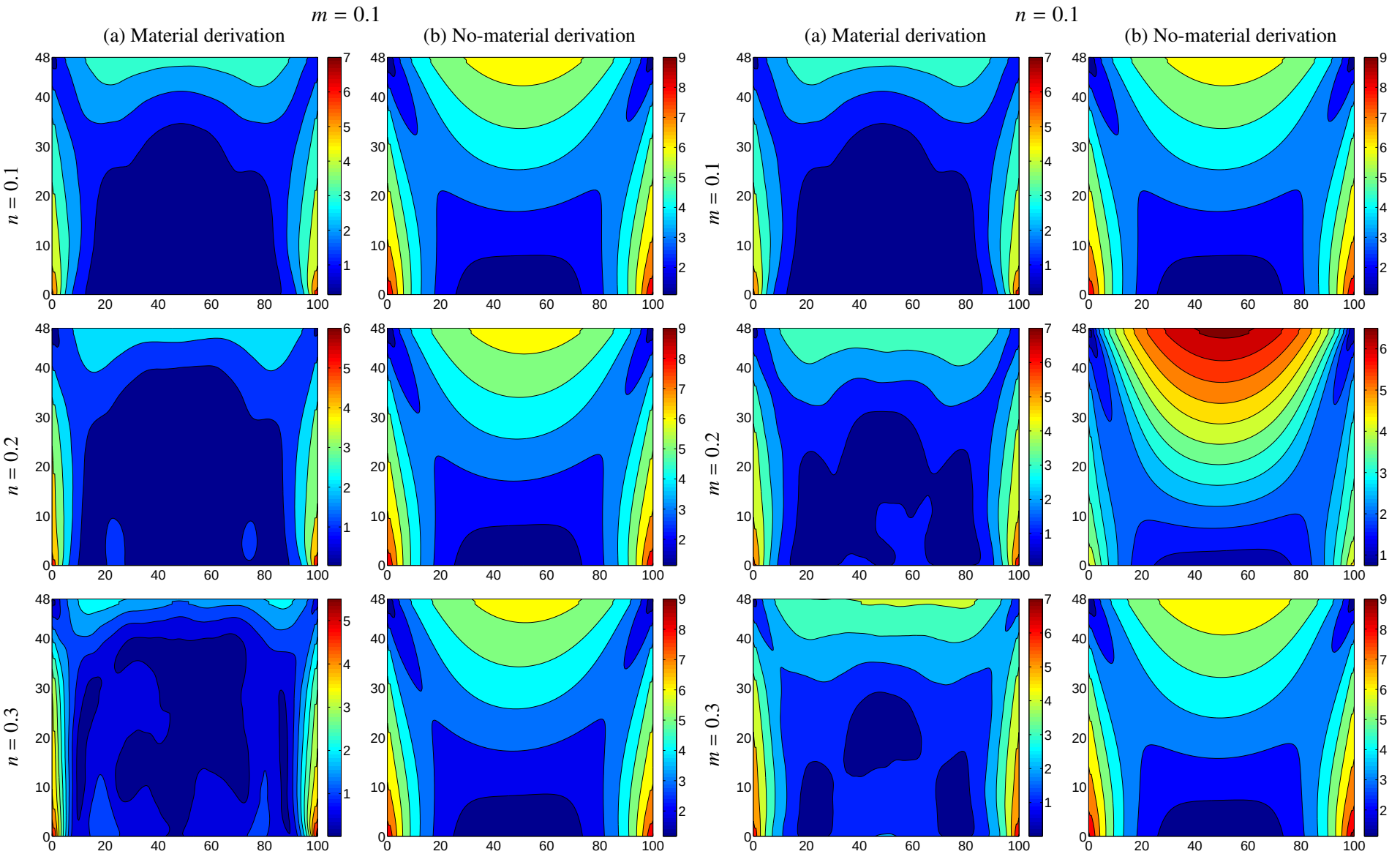

Figure 2. Effect of the compositional gradient exponents (n) and (m) in the $x-$ and $y-$directions on the equivalent strain $\varepsilon_{eqv}(x, y) \times 10^{-4}$ distributions in the upper plate based on the analyses with/without material derivation (apsis : x, (mm) and ordinate : y, (mm)).

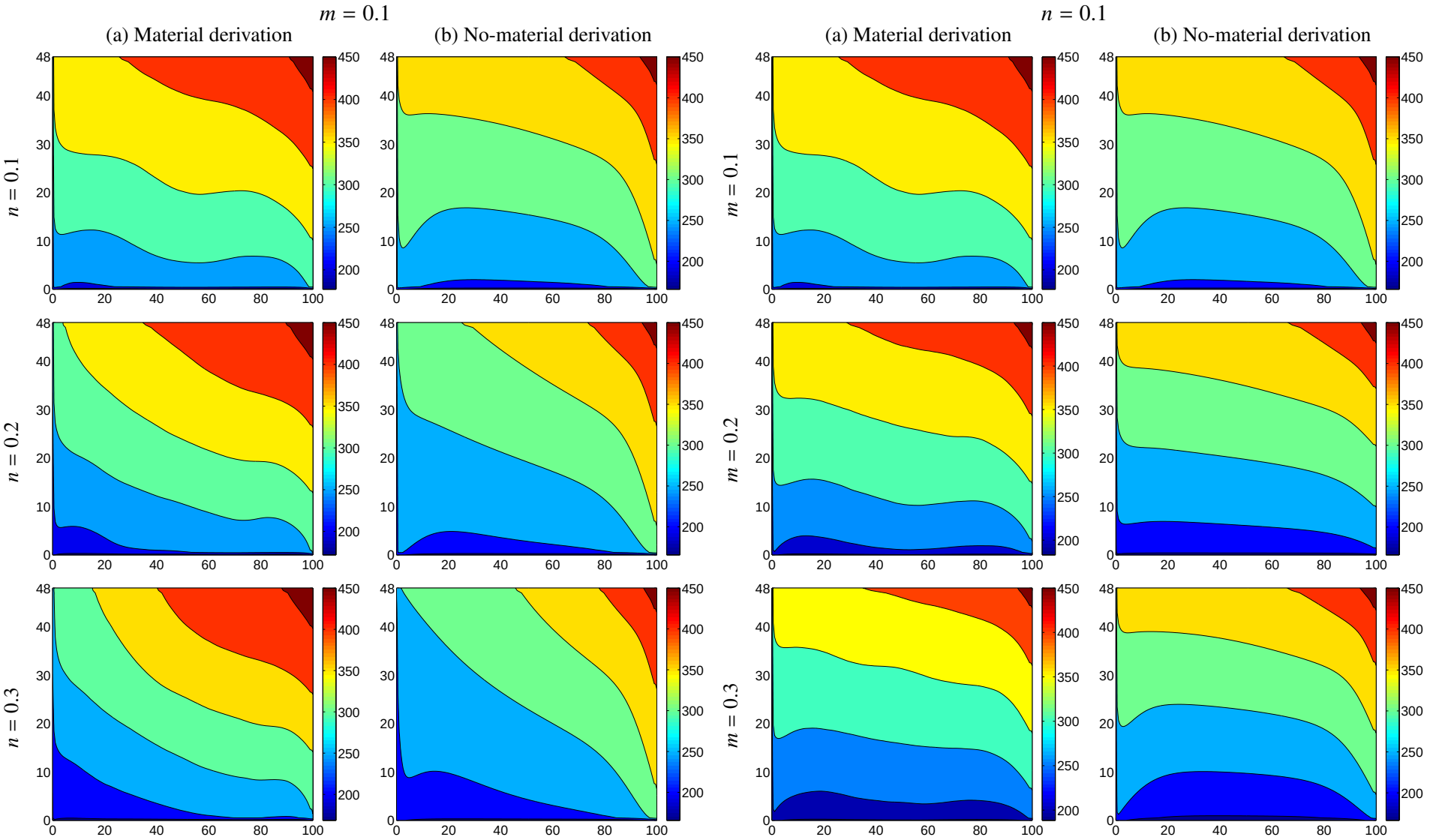

Figure 3. Effect of the compositional gradient exponents (n) and (m) in the $x-$ and $y-$directions on the equivalent stress $\sigma_{eqv}\,(x, y)$ distributions in the upper plate based on the analyses with/without material derivation (apsis : x, (mm) and ordinate : y, (mm)).

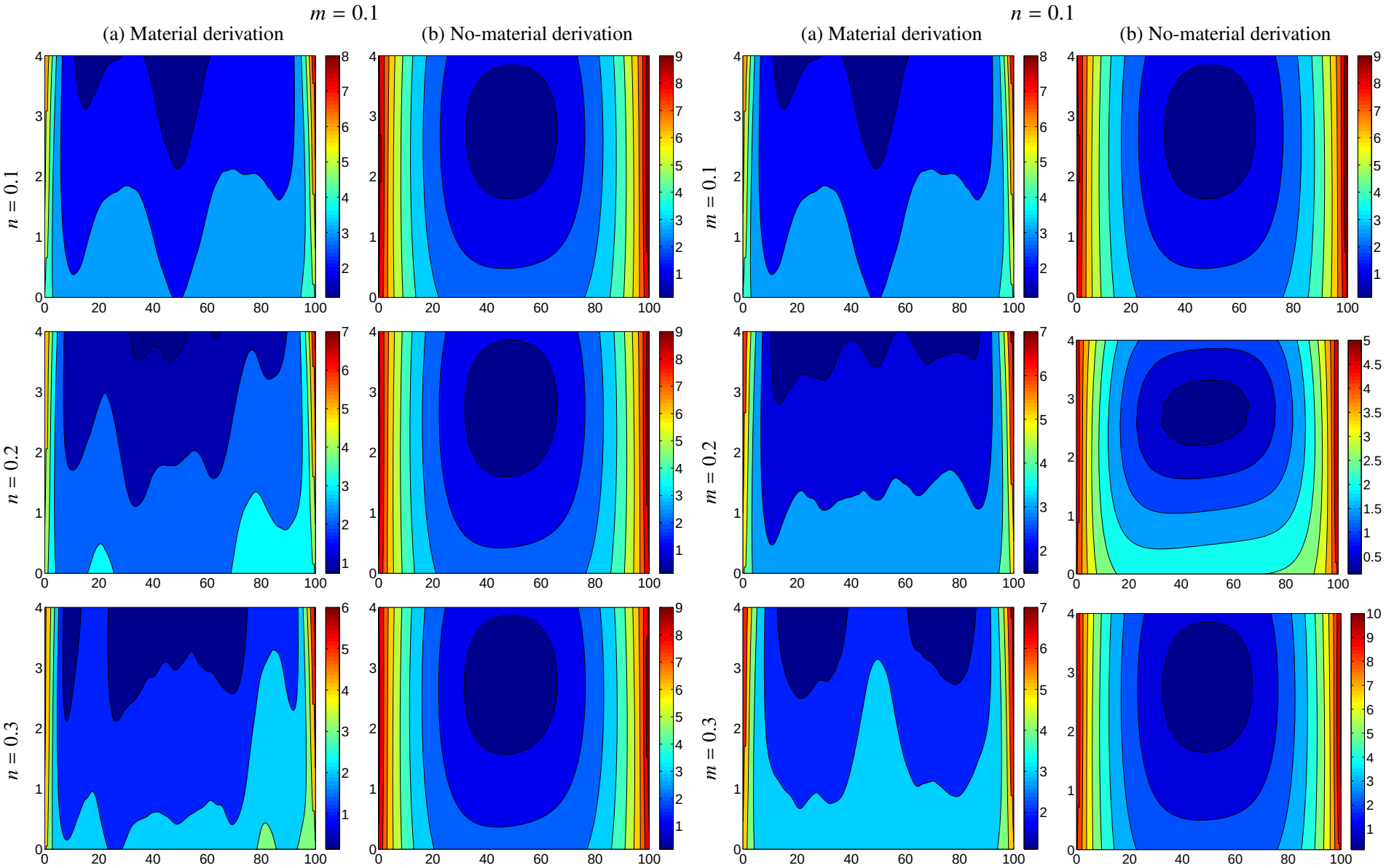

Figure 4. Effect of the compositional gradient exponents (n) and (m) in the $x-$ and $y-$directions on the equivalent strain $\varepsilon_{eqv}(x, y) \times 10^{-4}$ distributions in the adhesive layer based on the analyses with/without material derivation (apsis : x, (mm) and ordinate : y, (mm)).

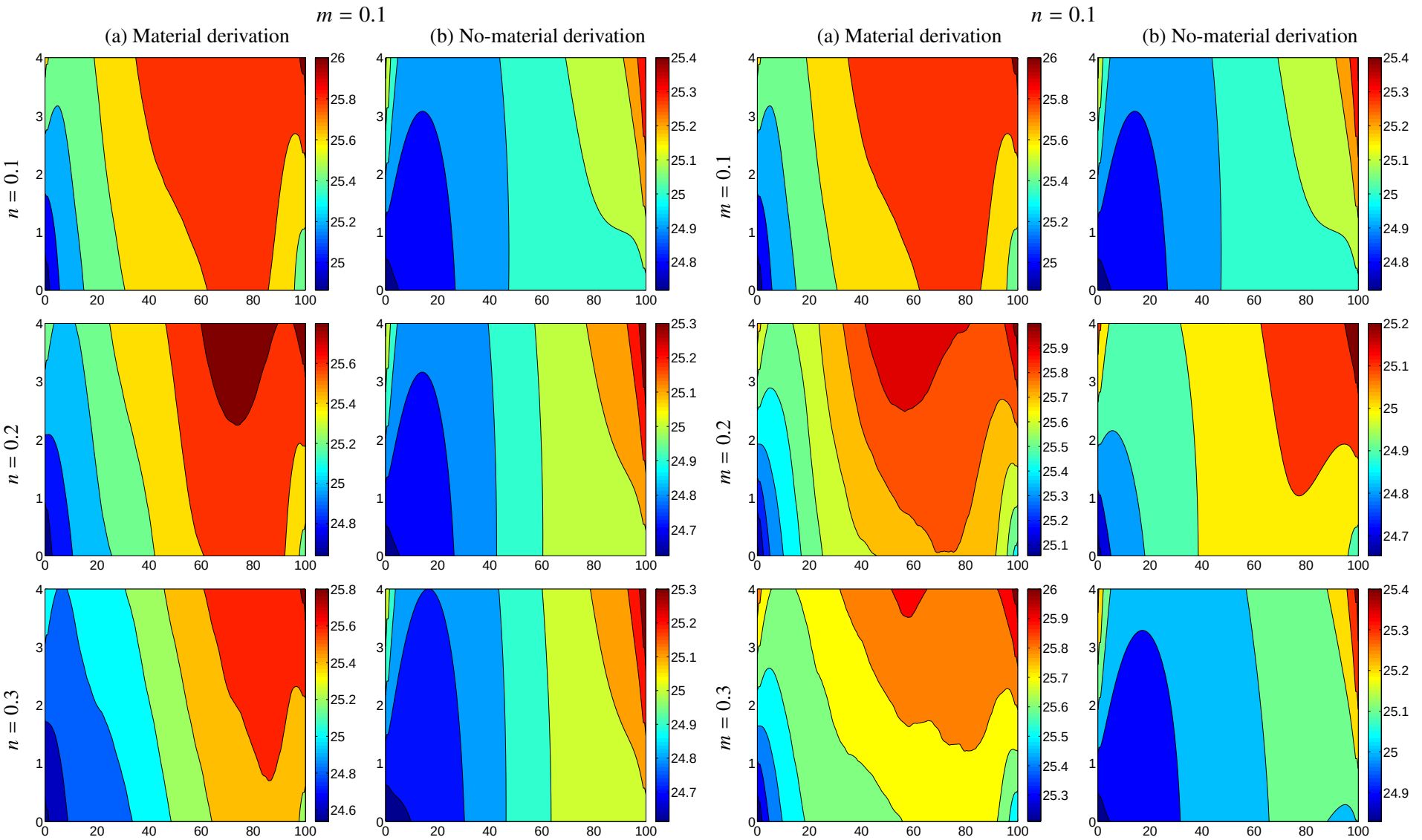

Figure 5. Effect of the compositional gradient exponents (n) and (m) in the $x-$ and $y-$directions on the equivalent stress $\sigma_{eqv}(x, y)$ distributions in the adhesive layer based on the analyses with/without material derivation (apsis : x, (mm) and ordinate : y, (mm)).

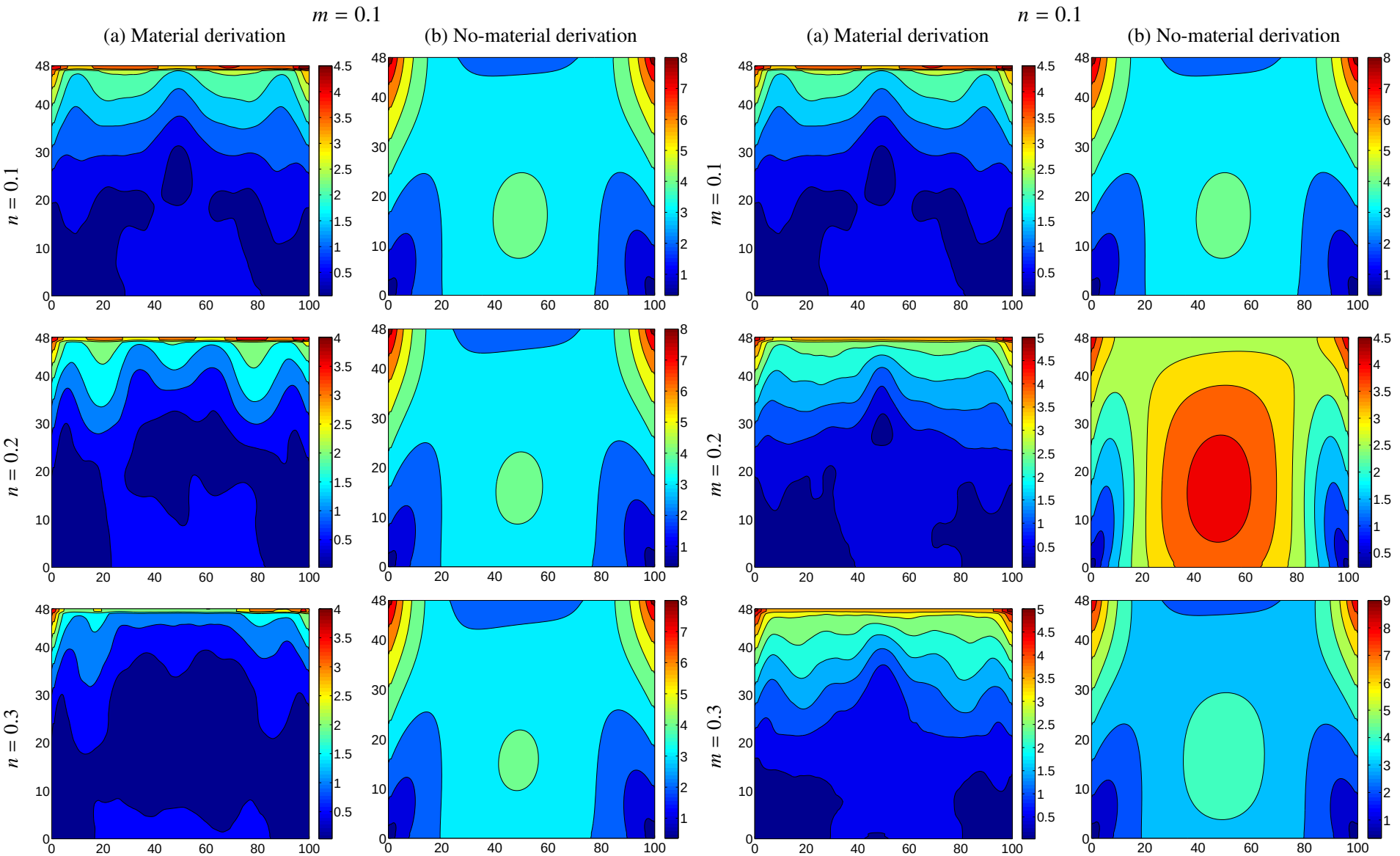

Figure 6. Effect of the compositional gradient exponents (n) and (m) in the $x-$ and $y-$directions on the equivalent strain $\varepsilon_{eqv}\,(x,y)\times 10^{-4}$ distributions in the lower plate based on the analyses with/without material derivation (apsis : x, (mm) and ordinate : y, (mm)).

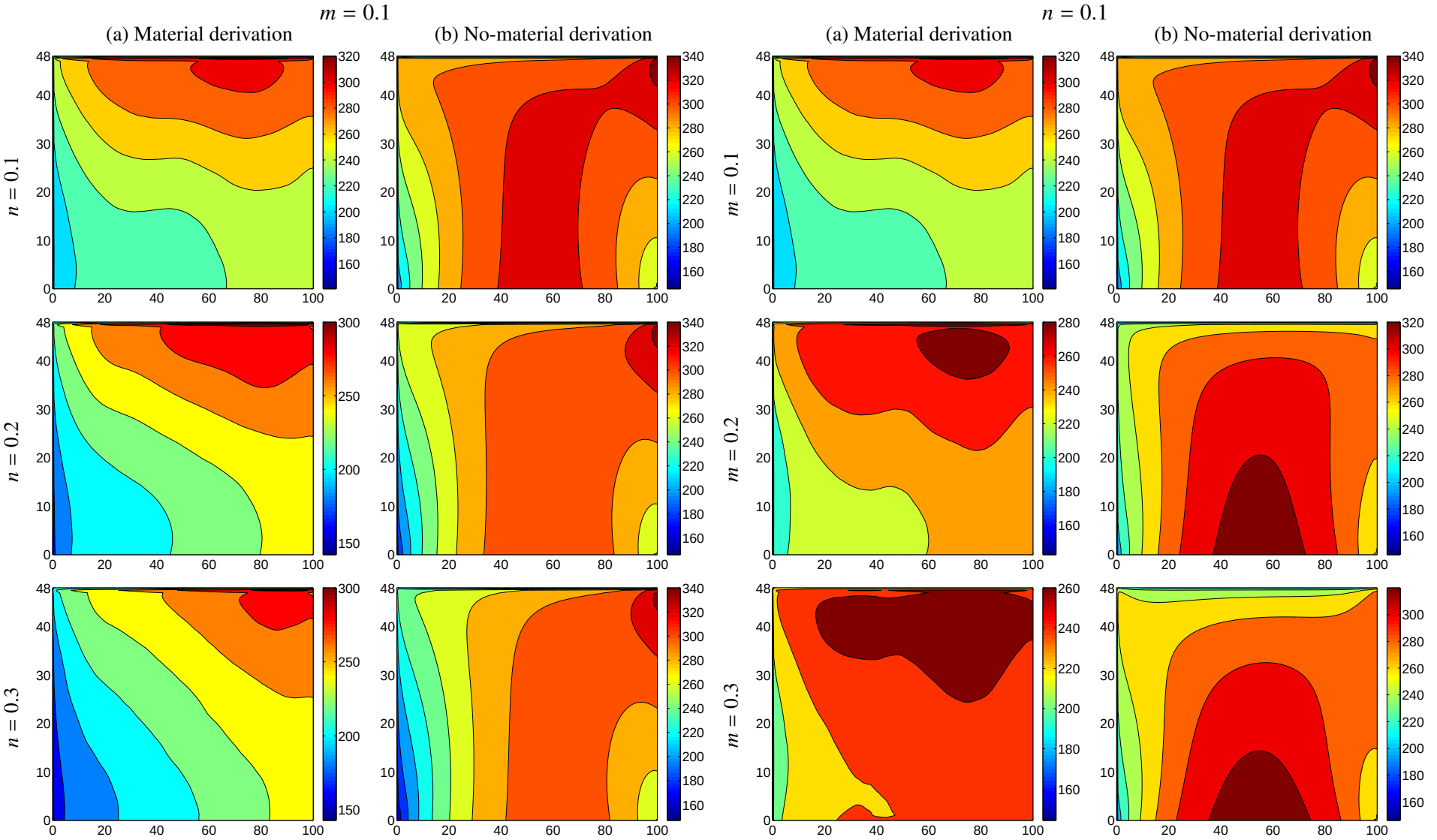

Figure 7. Effect of the compositional gradient exponents (n) and (m) in the $x-$ and $y-$directions on the equivalent stress $\sigma_{eqv}(x, y) \times 10^{-4}$ distributions in the lower plate based on the analyses with/without material derivation (apsis : x, (mm) and ordinate : y, (mm)).

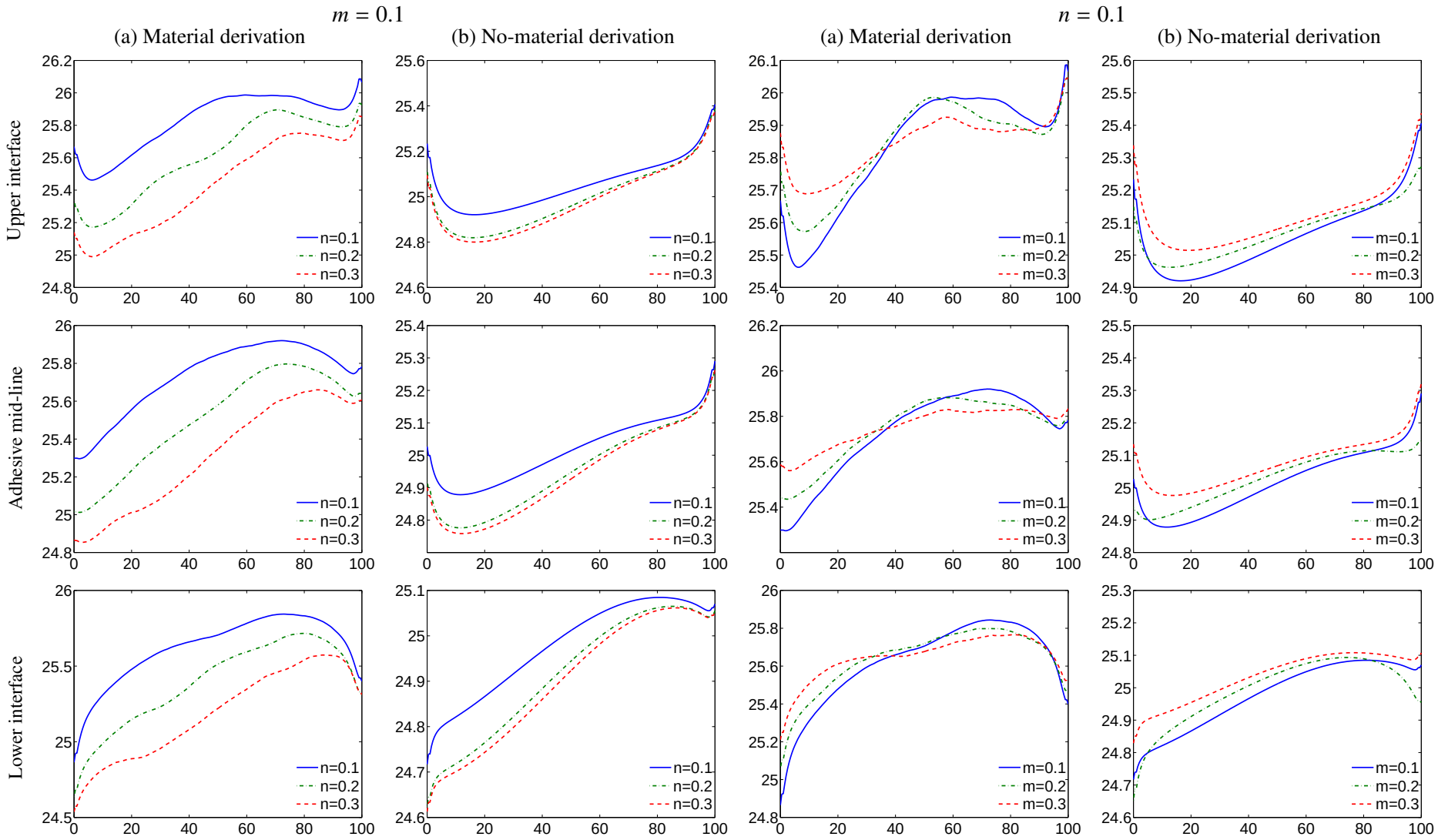

Figure 8. Effect of the compositional gradient exponents (n) and (m) in the $x-$ and $y-$directions on the equivalent stress $\sigma_{eqv}\,(x, y)$ distributions along the upper plate-adhesive interface, adhesive mid-line and the lower plate-adhesive interface based on the analyses with/without material derivation (apsis : x, (mm) and ordinate : σ_{eqv}, (MPa)).

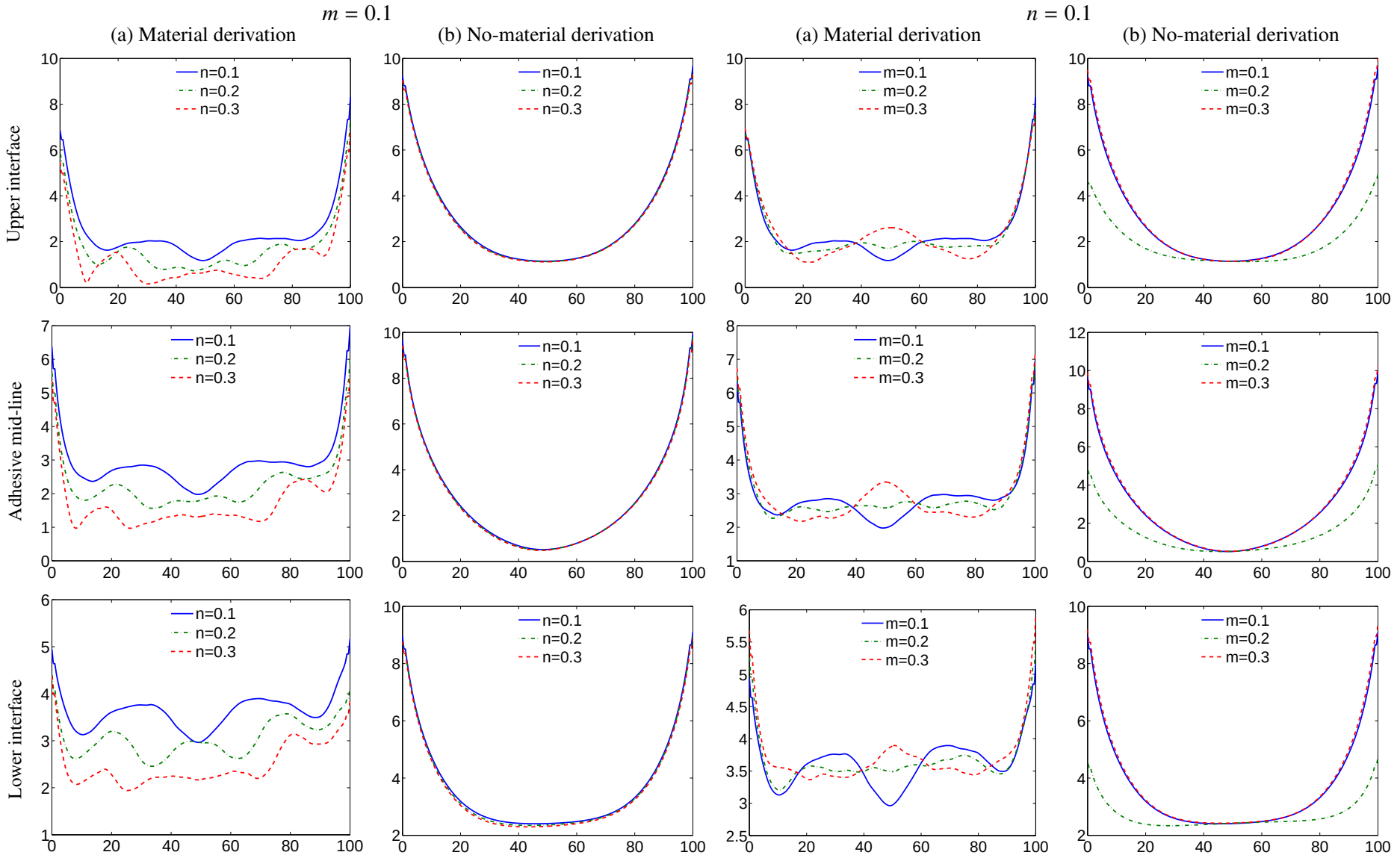

Figure 9. Effect of the compositional gradient exponents (n) and (m) in the $x-$ and $y-$directions on the equivalent strain $\varepsilon_{eqv}(x,y) \times 10^{-4}$ distributions along the upper plate-adhesive interface, adhesive mid-line and the lower plate-adhesive interface based on the analyses with/without material derivation (apsis : x, (mm) and ordinate : ε_{eqv}).

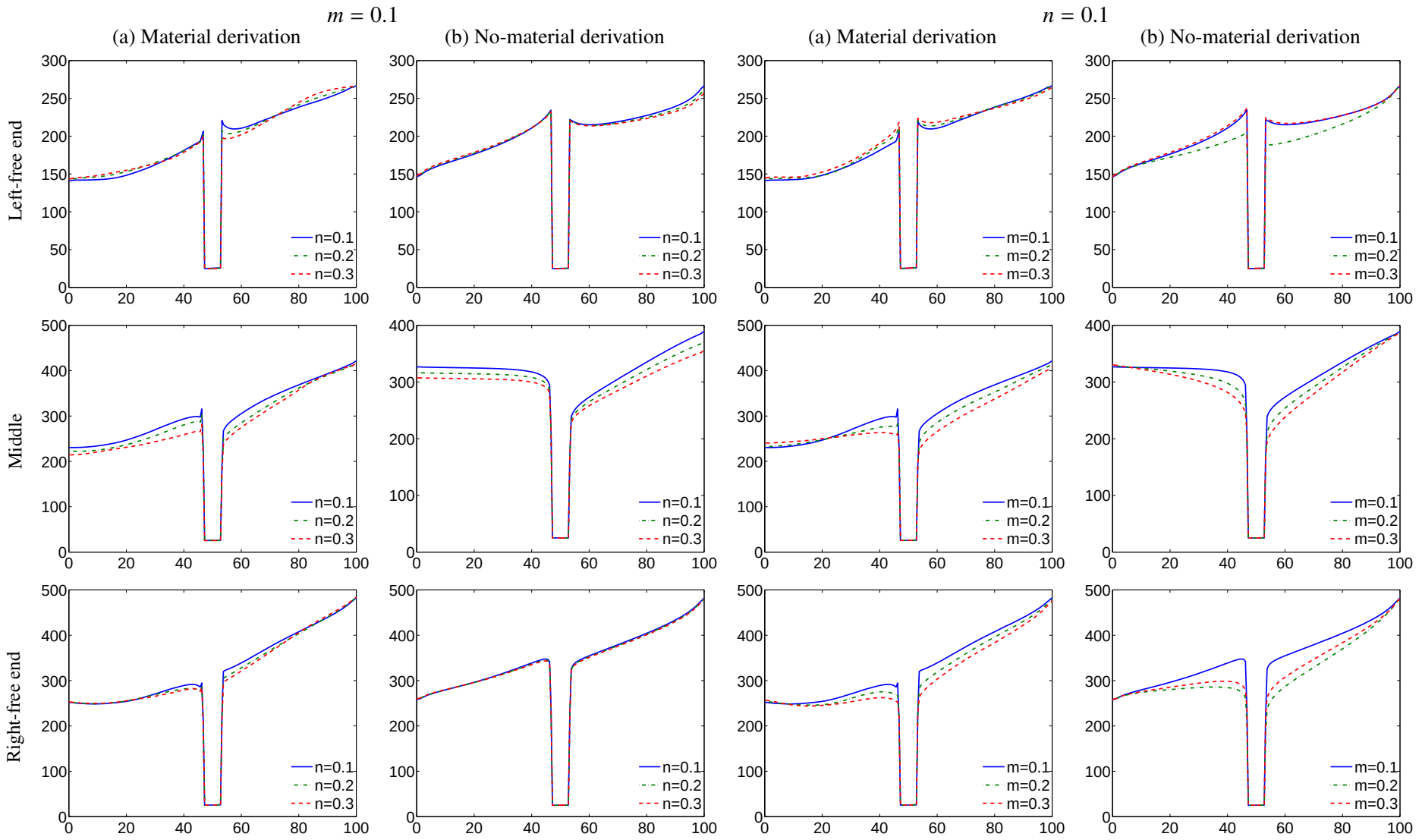

Figure 10. Effect of the compositional gradient exponents (n) and (m) in the $x-$ and $y-$directions on the equivalent stress $\sigma_{eqv}(x, y)$ distributions at the left-free edge, in the mid-line and at the right-free edge of the adhesive joint based on the analyses with/without material derivation (apsis : y, (mm) and ordinate : σ_{eqv}, (MPa)).

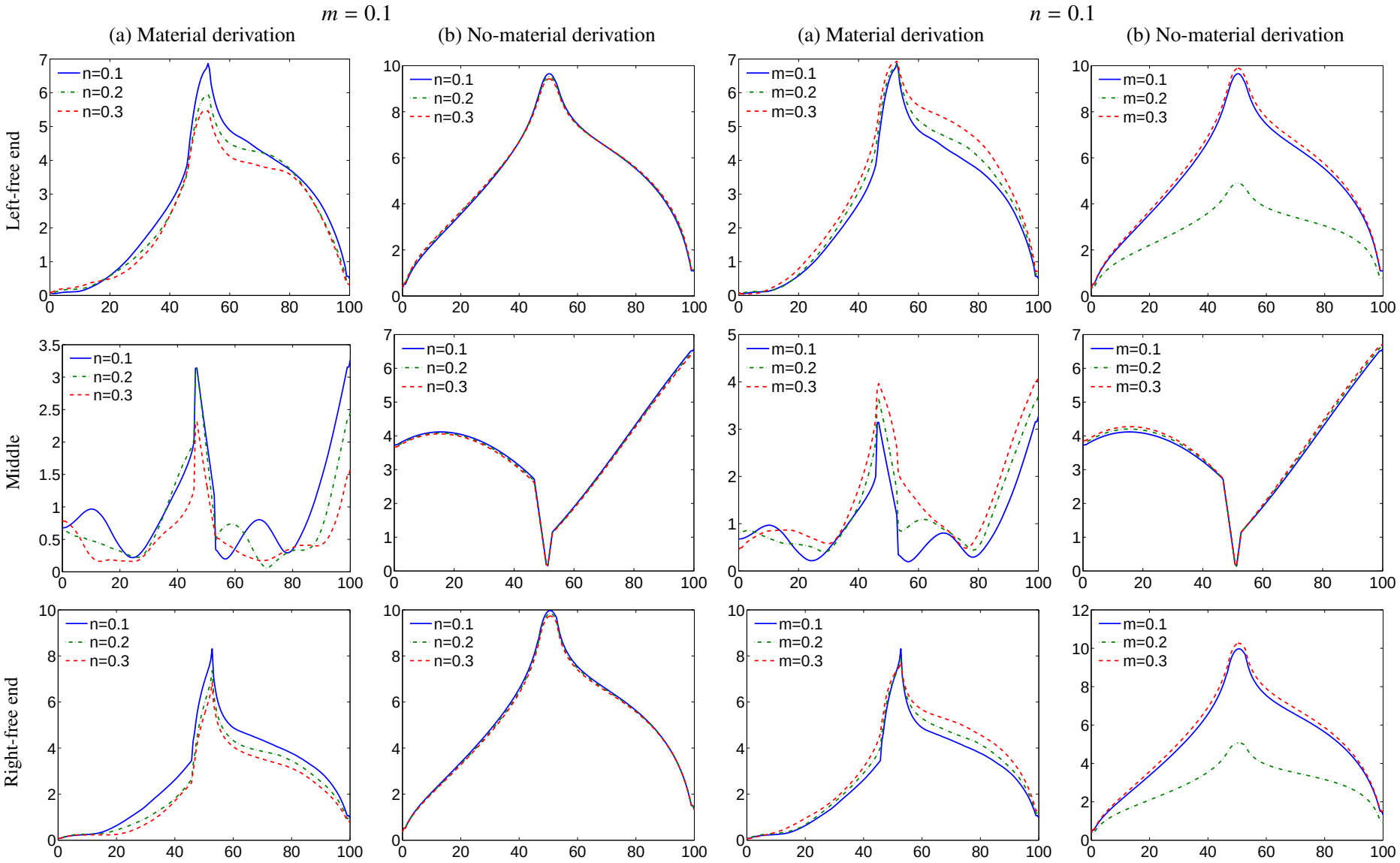

Figure 11. Effect of the compositional gradient exponents (n) and (m) in the $x-$ and $y-$directions on the equivalent strain $\varepsilon_{eqv}(x, y) \times 10^{-4}$ variations at the left-free edge, in the mid-line and at the right-free edge of the adhesive joint based on the analyses with/without material derivation (apsis : y, (mm) and ordinate : ε_{eqv}).